Fabrication of Nanoporous Nickel by Electrochemical Dealloying

Li Sun,† Chia-Ling Chien,‡ and Peter C. Searson*,†

Department of Materials Science and Engineering, Department of Physics and Astronomy, Johns Hopkins University, Baltimore, Maryland 21218

Received February 11, 2004. Revised Manuscript Received May 3, 2004

The etching of the more active component from a homogeneous alloy is important in corrosion reactions and has been exploited in the synthesis of high surface area nanoporous materials. In this paper we show that nanoporous films can be obtained by selective electrochemical etching of the more noble component in a system where the more active component is passivated. We demonstrate that nanoporous nickel films can be obtained by a two-step process involving electrodeposition of a homogeneous Ni_xCu_{1-x} alloy followed by electrochemical etching of the copper from the alloy. The composition, lattice parameter, saturation magnetization, and Curie temperature of the electrodeposited Ni_xCu_{1-x} alloys can be precisely controlled by varying the deposition conditions. Nanoporous nickel can be formed by electrochemically etching the copper from the alloy. The nanoporous structures are characterized by a three-dimensional network of interconnected pores and exhibit enhanced coercivity and reduced magnetic anisotropy. The morphology of the nanoporous nickel films is dependent on the initial composition of the Ni_xCu_{1-x} alloy.

Introduction

A difference in chemical potential between the elements in a homogeneous alloy can lead to selective etching of the more active component and the formation of a porous structure. This process is known as dealloying and is important in a wide range of corrosion reactions where etching of the more active component occurs under open circuit conditions. Examples of systems in which dealloying has been observed include Cu−Zn,[1] Cu−Au,[2,3] and Ag−Au.[4,5] The dealloying process has been exploited in materials synthesis in the fabrication of high surface area nanoporous electrodes,[6,7] nanoporous gold nanowires,[8] and nanoporous gold nanoshells.[9]

A nanoporous structure of a metal A is obtained by etching component B from a homogeneous, single-phase A_xB_{1-x} alloy. The pore size in the dealloyed structure is dependent on alloy composition. Thus, alloy systems that form a solid solution across the whole compositional range provide the maximum flexibility in tailoring the properties over a wide range. As described above, dealloying usually occurs by selective etching of the more active element.

Here we show for the first time the formation of a nanoporous structure by dealloying the more noble component. We demonstrate that nanoporous Ni films can be formed by a process involving electrodeposition of a homogeneous, single-phase Ni_xCu_{1-x} binary alloy followed by electrochemical etching of Cu from the alloy in the same solution. Cu and Ni are both fcc with similar lattice parameters and form a solid solution across the whole compositional range. The standard equilibrium potentials for the Cu^{2+}/Cu and Ni^{2+}/Ni couples are 0.34 V (SHE) and −0.257 V (SHE), respectively, and hence copper is thermodynamically more stable than nickel by 0.597 V.[10] However, the formation of a passive oxide film on nickel in sulfamate solutions allows the selective electrochemical etching of copper, the less noble component. These results show a general strategy for fabrication of nanoporous structures by electrochemical dealloying where the more active component is passivated and hence is kinetically rather than thermodynamically stable. This strategy is important, for example, in the fabrication of nanoporous structures from transition metal elements.

Experimental Section

The Ni_xCu_{1-x} alloy films were deposited from solution containing 1.6 M $Ni(H_2NSO_3)_2 \cdot 4H_2O$ and 0.1 M $CuSO_4 \cdot 5H_2O$ buffered to pH 2.5 with H_3BO_3. Electrochemical experiments were performed under ambient conditions in a three-electrode

* To whom correspondence should be addressed. E-mail: searson@jhu.edu.
† Department of Materials Science and Engineering.
‡ Department of Physics and Astronomy.

(1) Pickering, H. W.; Wagner, C. *J. Electrochem. Soc.* **1967**, *114*, 698−706.
(2) Fritz, J. D.; Pickering, H. W. *J. Electrochem. Soc.* **1991**, *138*, 3209−3218.
(3) Moffat, T. P.; Fan, F. R.; Bard, A. J. *J. Electrochem. Soc.* **1991**, *138*, 3224−3235.
(4) Forty, A. J. *Nature* **1979**, *282*, 597−598.
(5) Erlebacher, J. D.; Aziz, M. J.; Karma, A.; Dimitrov, N.; Sieradzki, K. *Nature* **2001**, *410*, 450−453.
(6) Ding, Y.; Erlebacher, J. D. *J. Am. Chem. Soc.* **2003**, *125*, 7772−7773.
(7) Katagiri, A.; Nakata, M. *J. Electrochem. Soc.* **2003**, *150*, C585−C590.
(8) Ji, C.; Searson, P. C. *J. Phys. Chem. B.* **2003**, *107*, 4494−4499.
(9) Sun, Y.; Xia, Y. *Nano Lett.* **2003**, *3*, 1569−1572.
(10) *Standard Potentials in Aqueous Solutions*; Bard, A. J., Parsons, R., Jordan, J., Eds.; Marcel Dekker: New York, 1985.

10.1021/cm0497881 CCC: $27.50 © 2004 American Chemical Society
Published on Web 07/10/2004

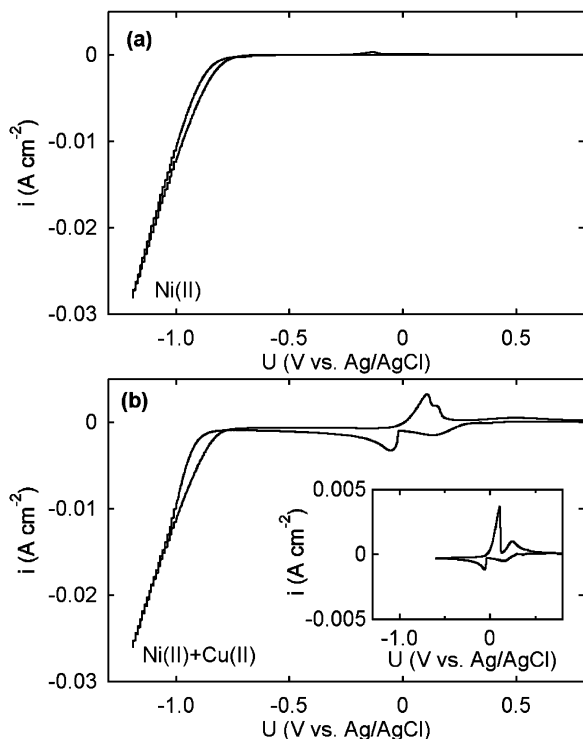

Figure 1. Current−voltage curves for (a) 1.6 M Ni(II) and (b) 1.6 M Ni(II) and 0.1 M Cu(II), on a gold electrode. The inset shows a current−voltage curve where the scan is reversed prior to the onset of nickel deposition. The scan rate was 20 mV s^{-1}. $U_{eq}(Cu^{2+}/Cu)$ = 0.081 V (Ag/AgCl) and $U_{eq}(Ni^{2+}/Ni)$ = −0.451 V (Ag/AgCl).

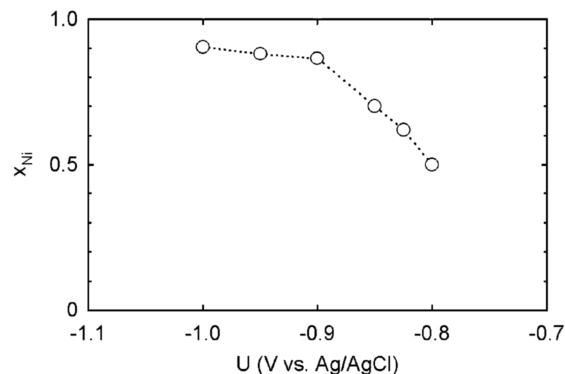

Figure 2. Mole fraction of nickel versus deposition potential for Ni_xCu_{1-x} films.

cell with a platinum counter electrode and a Ag/AgCl (3 M NaCl) reference electrode. All potentials are reported versus the Ag/AgCl reference (0.200 V vs SHE). Films were deposited onto 100-nm-thick (111) textured Au films sputtered on Si(100) wafers with a 5-nm Cr adhesion layer. The working electrode area was 1 cm^2.

Ni_xCu_{1-x} alloy films were deposited at constant potential in the range from −0.75 to −1.0 V. For comparison, pure Cu films were deposited at −0.3 V from the same solution. Pure Ni films were deposited from 1.6 M $Ni(H_2NSO_3)_2 \cdot 4H_2O$ solution at −1.0 V. In all cases the deposition charge was 3 C cm^{-2}. The deposition efficiency, determined from weight change experiments, was 0.95 at all deposition potentials. Taking into account the measured deposition efficiency, the deposition charge corresponds to a film thickness of 1.05 μm for copper and 0.97 μm for nickel.

The film composition was determined by auger electron spectroscopy. The structure of deposited films was determined by X-ray diffraction using a Cu Kα radiation (λ = 0.15406 nm). The diffraction patterns were calibrated using the Si(004) diffraction peak (2θ = 69.1729°). Magnetization hysteresis loops were recorded using a superconducting quantum interference device (SQUID) at low temperatures, and a vibrating sample magnetometer (VSM) at higher temperatures.

Results and Discussion

Figure 1a shows a current−voltage curve for 1.6 M Ni(II) solution. The onset potential for nickel deposition, at about −0.7 V, is about 300 mV negative to the equilibrium potential for the Ni^{2+}/Ni couple in this solution, which is U_{eq} = −0.451 V.[10] At more negative potentials, the nickel deposition current increases exponentially with potential. On the positive scan there is no stripping and only a small passivation peak is seen at about −0.1 V.[11] Figure 1b shows a current−voltage curve for solution containing 1.6 M Ni(II) and 0.1 M Cu(II). Reduction peaks associated with Cu(I) and Cu(0) are seen at 0.2 and −0.06 V, respectively.[12] In the potential range from −0.1 V to the onset of Ni deposition at about −0.70 V, the diffusion limited deposition of copper is the only reduction process. At more negative potentials, both Ni and Cu are deposited. On the positive scan, the characteristic peaks associated with Cu stripping are seen, with the main stripping peak at 0.105 V. The equilibrium potential for the Cu^{2+}/Cu couple in this solution is U_{eq} = 0.081 V.

The inset of Figure 1b shows a current−voltage curve in Ni(II) and Cu(II) solution with a negative scan limit of −0.6 V demonstrating that the deposition and stripping peaks at more positive potentials are associated with copper. These results show that Cu is selectively stripped from Ni_xCu_{1-x} alloys at positive potentials.

At potentials negative to the equilibrium potential for nickel, copper deposition is diffusion-limited and hence the rate is independent of potential, whereas the rate of nickel deposition increases with decreasing potential. As a result, the nickel concentration in the deposited film is expected to increase with decreasing potential. Figure 2 shows the composition of Ni_xCu_{1-x} films versus the deposition potential. The mole fraction of nickel increases from about x_{Ni} = 0.50 at a deposition potential of −0.8 V, to x_{Ni} = 0.91 at −1.0 V. Auger depth profiles confirmed that the composition was uniform throughout the film in all cases.

X-ray diffraction patterns for Ni_xCu_{1-x} films deposited at different potentials are shown in Figure 3a, along with diffraction patterns for pure Ni and pure Cu films. The diffraction spectra of all the Ni_xCu_{1-x} films show strong (111) texture with no evidence of other diffraction peaks. The diffraction peaks for pure Cu and pure Ni at 43.41° and 44.59°, respectively, correspond to lattice parameters of a_{Ni} = 0.3517 nm and a_{Cu} = 0.3607 nm, in good agreement with values reported in the literature.[13] As the deposition potential decreases from −0.8 to −1.0 V the Ni_xCu_{1-x} (111) peak shifts toward the Ni (111) peak corresponding to an increase in the mole

(11) Sato, N.; Okomoto, G. In *Comprehensive Treatise of Electrochemistry*; Conway, B. E., Yeager, E., White, R. E., Eds.; Plenum: New York, 1981; Vol. 4, pp 193−276.
(12) Zhou, M.; Myung, N.; Chen, X.; Rajeshwar, K. *J. Electroanal. Chem.* **1995**, *398*, 5−12.
(13) Joint Committee on Powder Diffraction Standards − International Centre for Diffraction Data, NIST, 2001.

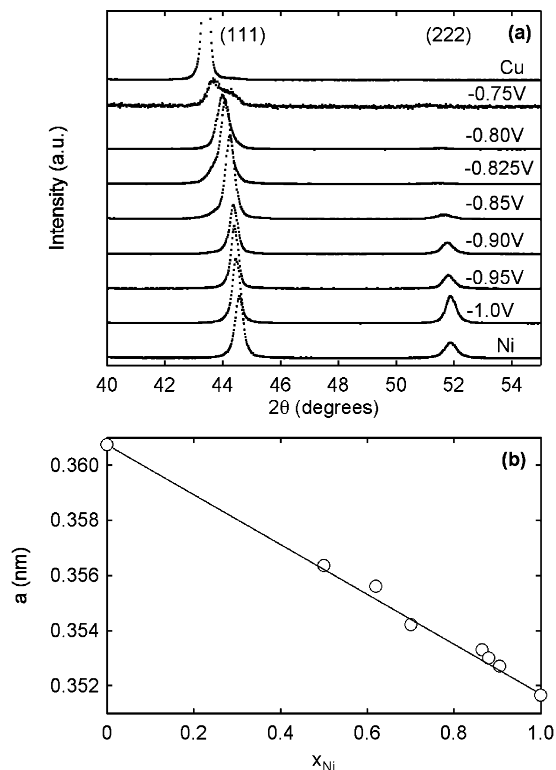

Figure 3. (a) X-ray diffraction patterns for Ni_xCu_{1-x} alloys. $2\theta = 44.59°$ for Ni(111) and $2\theta = 43.41°$ for Cu(111). (b) The lattice parameter obtained from the position of the (111) peak versus film composition determined from auger electron spectroscopy.

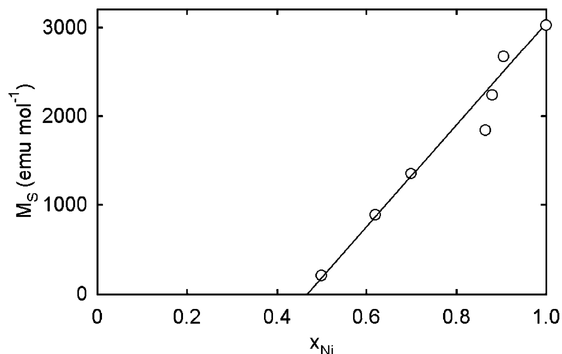

Figure 4. Saturation magnetization for electrodeposited Ni_xCu_{1-x} films versus film composition.

fraction of nickel in the film. Films deposited at −0.75 V or more positive potentials exhibited peak splitting indicating phase separation and hence the formation of an inhomogeneous alloy.

The lattice parameters of the Ni_xCu_{1-x} films calculated from the position of the (111) peak are plotted versus the film composition in Figure 3b. The linear dependence of the lattice parameter on mole fraction of nickel in the film according to Vegard's rule further confirms the formation of a homogeneous solid solution.

The magnetic properties of the Ni_xCu_{1-x} films show strong compositional dependence. Figure 4 shows the dependence of the saturation magnetization on film composition. For convenience we use units of emu per mole of nickel in the film. The saturation magnetization for pure nickel films deposited from Ni(II) solution was 3023 emu mol^{-1} at room temperature, corresponding to 95% of the bulk value (3191 emu mol^{-1}). With decreasing mole fraction of nickel in the films, the saturation magnetization decreases linearly as expected for a simple rule of mixtures. The alloy becomes paramagnetic at $x_{Ni} = 0.47$, in good agreement with results for bulk Ni_xCu_{1-x} alloys fabricated by casting.[14,15]

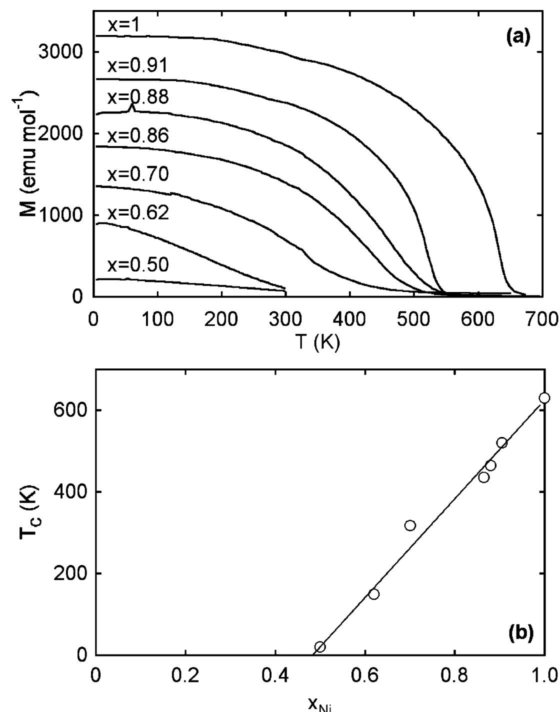

Figure 5. (a) Magnetization versus temperature curves as a function of film composition and (b) Curie temperature versus film composition.

The temperature dependence of the magnetization for different Ni_xCu_{1-x} film compositions is shown in Figure 5a. The Curie temperature, obtained from the *M*−*T* curves, is plotted versus the mole fraction of nickel in the film in Figure 5b. The Curie temperature for the pure nickel film was 631 K, which is identical to the value for bulk nickel.[16] The Curie temperature decreases linearly with decreasing mole fraction of nickel, as has been reported for bulk alloys.[14,15]

Nanoporous nickel films were produced by etching the copper from the Ni_xCu_{1-x} films at 0.5 V for 3 h. The films were etched immediately after deposition in the same solution. As described previously, nickel is passivated in this solution and hence copper can be selectively etched.

Figure 6 shows plan-view scanning electron microscope images of Ni_xCu_{1-x} films after dealloying. As can be seen from the images, the morphology of the films is dependent on the original composition of the alloy. Dealloying a $Ni_{0.86}Cu_{0.14}$ film results in the formation of surface pits up to about 100 nm in diameter. Dealloying the $Ni_{0.7}Cu_{0.3}$ film results in an interconnected network of pores 100−200 nm in diameter. After dealloying the $Ni_{0.62}Cu_{0.38}$ film, the morphology is irregular with a distribution of pores up to about 400 nm in diameter. Dealloying the $Ni_{0.5}Cu_{0.5}$ film results in the

(14) Ahern, S. A.; Martin, M. J. C.; Sucksmith, W. *Proc. Royal Soc. A* **1958**, *248*, 145−152.
(15) Robbins, C. G.; Claus, H.; Beck, P. A. *Phys. Rev. Lett.* **1969**, *22*, 1307−1310.
(16) Bozorth, R. M. *Ferromagnetism*; IEEE Press: New York, 1978.

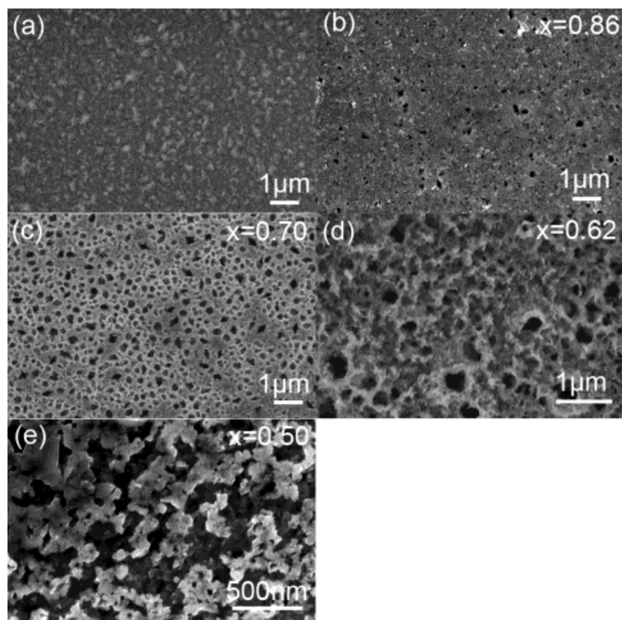

Figure 6. Plan view SEM images of (a) as-deposited film, and dealloyed films (b) $Ni_{0.86}Cu_{0.14}$, (c) $Ni_{0.70}Cu_{0.30}$, (d) $Ni_{0.62}Cu_{0.38}$, and (e) $Ni_{0.50}Cu_{0.50}$.

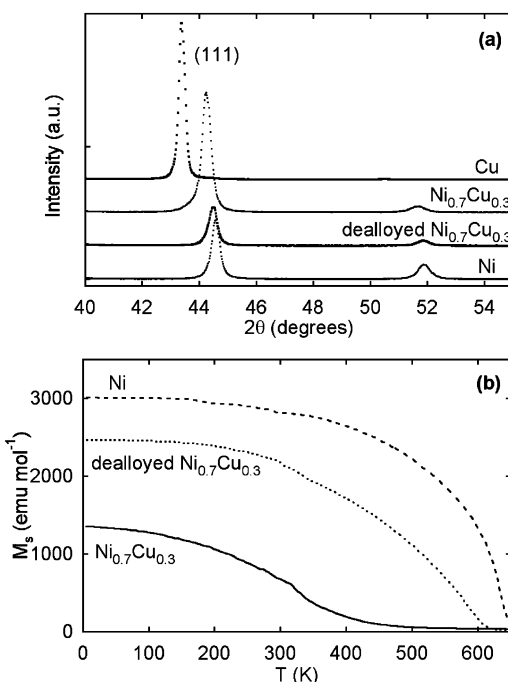

Figure 7. (a) X-ray diffraction patterns (b) and temperature dependence of the saturation magnetization for as-deposited and dealloyed $Ni_{0.70}Cu_{0.30}$ films.

formation of a porous structure with ligaments 100–200 nm in size. These irregular morphologies indicate that these structures do not exhibit significant coarsening due to passivation of the nickel and suggest that the mobility of nickel is relatively low.

Figure 7 shows X-ray diffraction patterns and magnetization versus temperature curves for $Ni_{0.7}Cu_{0.3}$ films before and after dealloying. The (111) diffraction peak for the $Ni_{0.7}Cu_{0.3}$ film after dealloying shifts to higher angle, close to the value for pure nickel. From the position of the (111) peak and Figure 3 we determine a residual mole fraction of copper in the dealloyed film of 0.074, illustrating that not all of the copper is removed from the film during etching. There is no peak broadening or peak separation indicating uniform etching of copper from the alloy.

The Curie temperature of the $Ni_{0.7}Cu_{0.3}$ film increases from 317.7 to 530 K after dealloying, as shown in Figure 7b. From Figure 5b, a Curie temperature $T_c = 530$ K corresponds to a mole fraction of copper of 0.08. The saturation magnetization of the dealloyed film was 2475 emu mol^{-1} which, from Figure 4, corresponds to a mole fraction of copper of 0.07. Thus, the mole fraction of copper in the dealloyed film obtained from the values of T_c and M_s are in excellent agreement with the value obtained from position of the (111) diffraction peak.

Magnetization hysteresis loops for a nickel film, a $Ni_{0.7}Cu_{0.3}$ film, and a dealloyed $Ni_{0.7}Cu_{0.3}$ film at room temperature with the applied field parallel and perpendicular to the film are shown in Figure 8. The $M-H$ loops for the nickel film and the $Ni_{0.7}Cu_{0.3}$ film are characteristic of thin films where the magnetic response is dominated by shape anisotropy (magnetostatic energy). With the applied field parallel to the film plane, the $M-H$ loops are relatively square with large remanence, characteristic of the magnetic easy axis. The magnetic response with the applied field perpendicular to the film plane is significantly sheared with very small remanence characteristic of the magnetic hard axis. In both cases the measured saturation field is close to $4\pi M_s$ as expected for a thin film ($4\pi M_s = 6095$ Oe for Ni and $4\pi M_s = 4270$ Oe for $Ni_{0.7}Cu_{0.3}$).[17,18] The coercivity of the dealloyed film ($H_c = 110$ Oe) is larger than that for the as-deposited film ($H_c = 50$ Oe).

The $M-H$ loops for the dealloyed film with the field parallel or perpendicular to the film plane are similar, consistent with the formation of an isotropic nanoporous structure. The saturation field perpendicular to the film plane is significantly smaller than $4\pi M_s$ and the in-plane saturation field also increases significantly compared to that of the as-deposited films.

Figure 9 shows $M-H$ curves for three film compositions, before and after dealloying. The differences between the $M-H$ curves before and after dealloying become more pronounced with increasing volume fraction of copper, reflecting the larger compositional changes on dealloying. For $x_{Ni} = 0.86$ and $x_{Ni} = 0.70$, the $M-H$ curves after dealloying exhibit a small increase in remanence and coercivity. For $x_{Ni} = 0.62$, the $M-H$ loop after dealloying is square with relatively high remanence and coercivity.

The coercivity of the dealloyed films increases with decreasing mole fraction of nickel in the as-deposited alloy, as shown in Figure 10. A similar enhancement in H_C has been reported for ferromagnetic network structures[19–21] and can be attributed to the domain wall pinning caused by the nonuniform structure. As can be seen from the SEM images in Figure 6, the porosity increases with decreasing mole fraction of nickel in the as-deposited film. At the same time, the feature sizes

(17) The values of $4\pi M_s$ were obtained from $M_s = 485$ emu cm^{-3} for nickel and $M_s = 340$ emu cm^{-3} for $Ni_{0.7}Cu_{0.3}$.

(18) Cullity, R. D. *Introduction to Magnetic Materials*; Addison-Wesley: Reading, MA, 1972.
(19) Barnard, J. A.; Fujiwara, H.; Inturi, V. R.; Jarratt, J. D.; Scharf, T. W.; Weston, J. L. *Appl. Phys. Lett.* **1996**, *69*, 2758–2760.
(20) Liu, K.; Chien, C. L. *IEEE Trans. Magn.* **1998**, *34*, 1021–1023.
(21) Sun, L.; Ding, Y.; Chien, C. L.; Searson, P. C. *Phys. Rev. B* **2001**, *64*, 184430–184434.

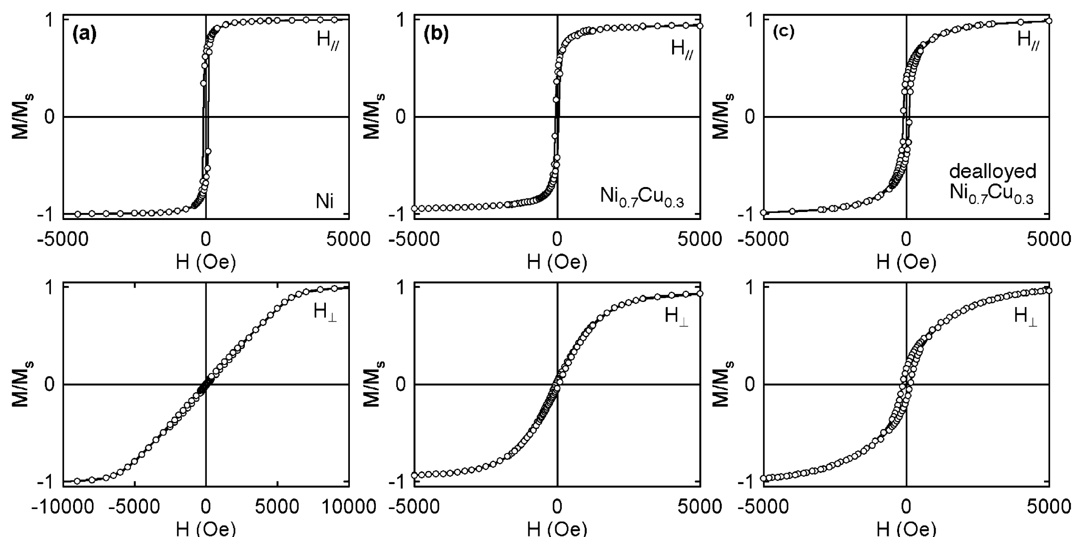

Figure 8. Room-temperature *M*−*H* curves for: (a) a Ni film, (b) an as-deposited $Ni_{70}Cu_{30}$ film, and (c) a dealloyed $Ni_{70}Cu_{30}$ film with the applied magnetic field parallel to the film plane (left panel), and perpendicular to the film plane (right panel).

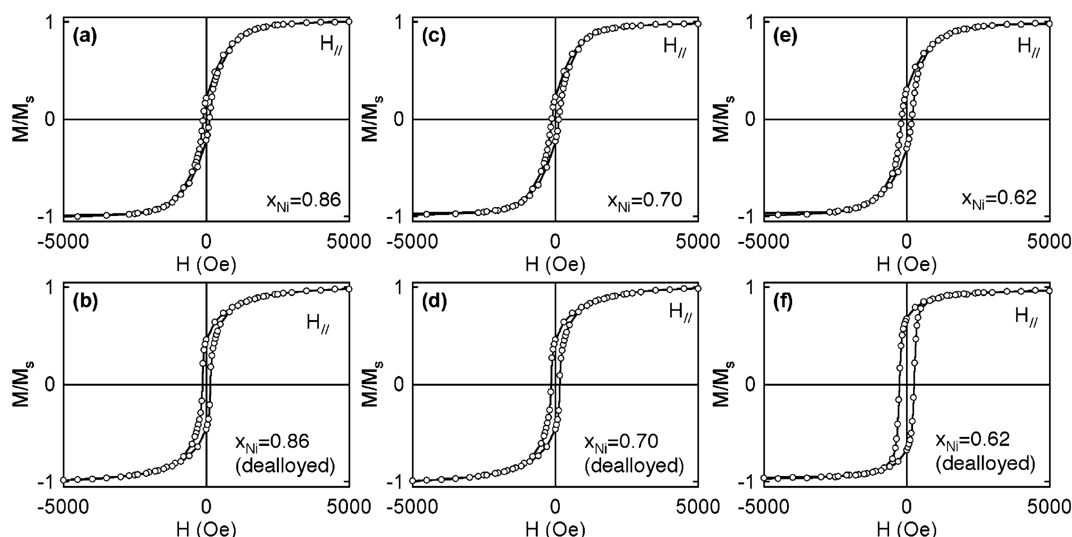

Figure 9. *M*−*H* curves for: (a) $Ni_{70}Cu_{30}$ film, (b) dealloyed $Ni_{70}Cu_{30}$ film, (c) $Ni_{70}Cu_{30}$ film, (d) dealloyed $Ni_{70}Cu_{30}$ film, (e) $Ni_{70}Cu_{30}$ film, (f) dealloyed $Ni_{70}Cu_{30}$ film. All measurements were performed at 5 K with the applied magnetic field parallel to the film plane.

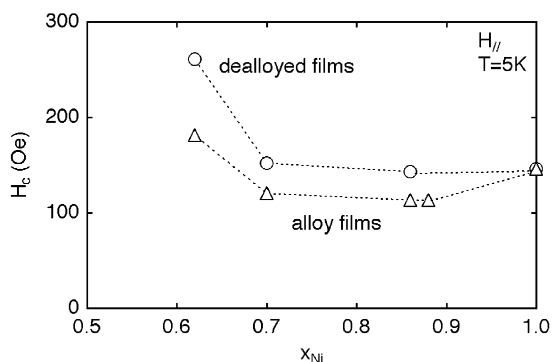

Figure 10. Dependence of coercivity on film composition for as-deposited and dealloyed films. All measurements were performed at 5 K with the applied magnetic field parallel to the film plane.

of the nickel ligaments decrease resulting in an increase in the coercivity.

In summary, we have shown that nanoporous films can be obtained by selective electrochemical etching of the more noble component in a system where the more active component is passivated. We have demonstrated that nanoporous nickel films can be obtained by a two-step process involving electrodeposition of a homogeneous Ni_xCu_{1-x} alloy followed by electrochemical etching of the copper from the alloy. The composition, lattice parameter, saturation magnetization, and Curie temperature of the electrodeposited Ni_xCu_{1-x} alloys can be precisely controlled by varying the deposition conditions. Nanoporous nickel can be formed by electrochemically etching the copper from the alloy. The nanoporous structures are characterized by a three-dimensional network of interconnected pores and exhibit enhanced coercivity and magnetic anisotropy. The morphology of the nanoporous nickel films is dependent on the initial composition of the Ni_xCu_{1-x} alloy.

Acknowledgment. This work was supported by the JHU MRSEC (NSF Grant DMR00-80031).

CM0497881